Fine-Structure Qubit Encoded in Metastable Strontium Trapped in an Optical Lattice

S. Pucher,[1,2] V. Klüsener,[1,2] F. Spriestersbach,[1,2] J. Geiger,[1,2] A. Schindewolf,[1,2,3] I. Bloch,[1,2,3] and S. Blatt[1,2,3,*]

[1]*Max-Planck-Institut für Quantenoptik, 85748 Garching, Germany*

[2]*Munich Center for Quantum Science and Technology, 80799 München, Germany*

[3]*Fakultät für Physik, Ludwig-Maximilians-Universität München, 80799 München, Germany*

(Received 19 January 2024; accepted 11 March 2024; published 11 April 2024)

We demonstrate coherent control of the fine-structure qubit in neutral strontium atoms. This qubit is encoded in the metastable $^3P_2$ and $^3P_0$ states, coupled by a Raman transition. Using a magnetic quadrupole transition, we demonstrate coherent state initialization of this THz qubit. We show Rabi oscillations with more than 60 coherent cycles and single-qubit rotations on the μs scale. With spin echo, we demonstrate coherence times of tens of ms. Our results pave the way for fast quantum information processors and highly tunable quantum simulators with two-electron atoms.

DOI: 10.1103/PhysRevLett.132.150605

Neutral atoms are a promising quantum computing [1] and quantum simulation [2] platform due to their long coherence times and highly scalable architecture [3,4]. Two-electron atoms in particular have gained increasing attention as their rich level structure offers multiple opportunities to encode high-quality qubits. Coupling a ground and a metastable state via an optical clock transition has enabled the observation of exceptionally long coherence times [5] and direct access to Rydberg states [6]. However, relying on an ultranarrow optical transition limits operating speed and poses challenges due to an inherent sensitivity to atomic motion and laser phase noise [7].

Faster and more robust qubit rotations can be achieved by coupling two states with a lower energy splitting using a coherent Raman transition [8]. Such a coupling scheme has been successfully implemented between nuclear spin states in fermionic isotopes of Yb [9,10] and Sr [11]. This nuclear-spin qubit led to the experimental demonstrations of high-fidelity gates [12], erasure conversion [13], and midcircuit operations [9,10,14]. Recently, a complementary encoding of information in electronic degrees of freedom provided by metastable fine-structure states has been proposed [15,16], similar to schemes that have been implemented in ions [17,18].

In contrast to nuclear spin states, which require a magnetic field to induce a qubit splitting typically in the kilohertz regime [8,11], the fine-structure states have a natural frequency splitting on the terahertz scale. Although this splitting makes it more challenging to achieve state-insensitive trapping conditions, it can be advantageous for state preparation and readout, as energy selectivity rather than polarization selectivity can be leveraged [7]. In

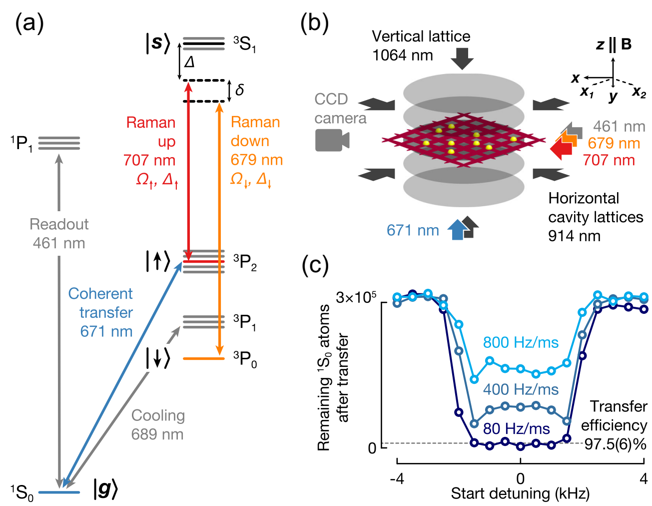

FIG. 1. Level scheme, schematic of experimental setup, and coherent state initialization. (a) Relevant ^{88}Sr energy levels. The fine-structure qubit is encoded in the metastable states $|^3P_2, m_J = 0\rangle$ and $|^3P_0, m_J = 0\rangle$, which are coupled via a two-photon Raman transition with a one-photon detuning Δ from $|^3S_1, m_J = 0\rangle$. The 689 and 461-nm light is used for cooling and imaging of the atoms, respectively. (b) Schematic of the experimental setup. Atoms are trapped in a horizontal (vertical) lattice formed at 914 nm (1064 nm). The magnetic bias field and the 671-nm state-preparation beam point along the z axis. The Raman beams and the imaging beam propagate along the x axis. (c) Coherent transfer of atoms from $|g\rangle$ to $|\uparrow\rangle$ using a Landau-Zener sweep with an efficiency of up to 97.5(6)%. The transfer-laser frequency is swept over 4 kHz with the indicated ramp speeds.

combination with the existing optical and nuclear qubits, this novel fine-structure qubit can unlock the full potential of the level scheme, leading to new functionalities such as optical qutrits [19], single-photon transition to Rydberg states with fast qubit rotations, and midcircuit readout operations.

Here, we experimentally demonstrate core capabilities of a fine-structure qubit using Sr atoms trapped in an optical lattice. As shown in Fig. 1(a), our qubit is encoded in the metastable triplet states $|\uparrow\rangle = |5s5p\,^3P_2, m_J = 0\rangle$ and $|\downarrow\rangle = |5s5p\,^3P_0, m_J = 0\rangle$, which are separated by about 17 THz in frequency. These states are coupled via a two-photon Raman transition through the triplet state $|s\rangle = |5s6s\,^3S_1, m_J = 0\rangle$. We demonstrate fast two-photon Rabi oscillations with frequencies up to $2\pi \times 400$ kHz and study their decoherence mechanisms. We show proof-of-principle read-out methods with about 96% detection efficiency that can be used for midcircuit readout. Finally, we investigate the coherence of the fine-structure qubit with Ramsey and spin-echo measurements.

The experimental setup is illustrated in Fig. 1(b). We load about 10^5 ^{88}Sr atoms into a 3D optical lattice [20]. In the horizontal direction, the atoms are trapped using laser light with a wavelength of 914 nm, which forms an optical lattice inside an enhancement cavity [21]. A retroreflected laser beam at 1064 nm generates the vertical lattice. After loading the atoms into the lattice, we perform resolved sideband cooling on the $^1S_0$–$^3P_1$ transition at a horizontal (vertical) lattice depth of $150E_{\rm rec}$ ($270E_{\rm rec}$), where $E_{\rm rec} = h^2/(2m\lambda_l^2)$ is the lattice photon recoil energy for an atom with mass m at the corresponding lattice wavelength λ_l, and h denotes the Planck constant. The trap depth corresponds to a horizontal (vertical) trap frequency of 65 kHz (68 kHz). We typically achieve temperatures of about 2.5 μK [20]. To initialize the qubit in $|\uparrow\rangle$, we coherently excite the atoms from the ground state $|g\rangle = |5s^2\,^1S_0\rangle$ to $|\uparrow\rangle$ using the magnetic field and lattice parameters from Ref. [20]. To achieve a robust state preparation, we perform a Landau-Zener sweep with a typical transfer efficiency of 97.5(6)%, as shown in Fig. 1(c) [22]. The same sweep is also used for state-selective readout of $|\uparrow\rangle$. The transfer efficiency could likely be further improved by more adiabatic sweeps, achievable, for example, with higher Rabi frequencies on the $|g\rangle$–$|\uparrow\rangle$ transition.

After state preparation, we set the magnetic field to 20 G, oriented along the z direction, corresponding to a Zeeman splitting of 42 MHz in the $^3P_2$ manifold, which helps to isolate the $m_J = 0$ state. We refer to the Raman laser beams driving the $|\uparrow\rangle$–$|s\rangle$ and the $|s\rangle$–$|\downarrow\rangle$ transition as the up and down lasers, respectively. They are both π polarized and copropagate in the x direction to minimize momentum transfer, with a Lamb-Dicke parameter of 0.01. We stabilize the laser frequencies to a shared optical reference cavity to ensure phase stability between the lasers. To suppress spontaneous decay from $|s\rangle$, we can detune the Raman lasers from the atomic transition frequencies by the one-photon detuning $\Delta = \Delta_\uparrow \approx \Delta_\downarrow$, where $\Delta_\uparrow$ and $\Delta_\downarrow$ are the detunings of the up laser and the down laser, respectively. The two-photon detuning $\delta = \Delta_\uparrow - \Delta_\downarrow$ is typically set to zero.

To achieve long coherence times within the Λ system, it is necessary to mitigate differential light shifts of the qubit states. The nonspherical $|\uparrow\rangle$ state features a tensor polarizability which allows tuning its light shift relative to the light shift of $|\downarrow\rangle$ by tilting the linear polarization of the trapping light field with respect to the magnetic quantization axis [19]. For the horizontal 914-nm lattice, we find the so-called "magic" trapping condition where the differential polarizability between $|\uparrow\rangle$ and $|\downarrow\rangle$ vanishes, close to the theoretically predicted angle of about 79°. For the vertical 1064-nm lattice no such magic angle exists and a residual differential polarizability on the percent level remains [22]. To minimize the differential light shift, we reduce the vertical lattice depth to about $27E_{\rm rec}$, corresponding to about 3 μK, and choose its polarization to be orthogonal to the magnetic field. The gravitational tilt of the vertical lattice helps to suppress tunneling and collisions, which are negligible on our experimental timescales [28,29].

To characterize the Λ system $|\uparrow\rangle$–$|s\rangle$–$|\downarrow\rangle$ containing the qubit subspace, we perform Autler-Townes spectroscopy. With this method, we calibrate the Rabi frequencies and demonstrate coherent population trapping to reveal the presence of coherence in the system. First, we resonantly couple $|\downarrow\rangle$ and $|s\rangle$ by applying the down laser with variable power $P_\downarrow$. The resulting splitting is given by the Rabi frequency $\Omega_\downarrow \propto \sqrt{P_\downarrow}$ of the down-laser field [30]. We probe this splitting by scanning the detuning $\Delta_\uparrow$ at $P_\uparrow = 30$ μW, as illustrated in Fig. 2(a). Readout is performed via detection of atoms that are excited from $|\uparrow\rangle$ to $|s\rangle$ and subsequently decay through $^3P_1$ into $|g\rangle$. A fit of the data results in $\Omega_\downarrow/\sqrt{P_\downarrow} = 2\pi \times 19.3(1)\ \mathrm{MHz}/\sqrt{\mathrm{mW}}$.

Next, we prepare the atoms in $|\downarrow\rangle$ and repeat the measurement with exchanged roles of the laser fields. We use $P_\downarrow \approx 220$ nW and find $\Omega_\uparrow/\sqrt{P_\uparrow} = 2\pi \times 24.3(2)\ \mathrm{MHz}/\sqrt{\mathrm{mW}}$, see Fig. 2(b). Finally, to observe coherent population trapping [32–34], we reduce the power in both laser fields significantly to about 10 nW. At the two-photon resonance we observe a narrow dip in the excitation spectrum, as shown in Fig. 2(c). A Lorentzian fit yields a full width at half maximum of $2\pi \times 0.71(19)$ kHz, four orders of magnitude narrower than the excited state's inverse lifetime $2\pi \times 11$ MHz [35]. This feature demonstrates the presence of coherence in the Λ system.

We now demonstrate coherent control of the fine-structure qubit by performing two-photon Rabi oscillations. To this end, we prepare the atoms in $|\uparrow\rangle$, set the one-photon detuning to $\Delta \approx -2\pi \times 6$ GHz, and tune the lasers to the two-photon resonance $\delta = 0$. Both laser fields have a Rabi frequency of $\Omega_\uparrow = \Omega_\downarrow \approx 2\pi \times 36$ MHz to minimize

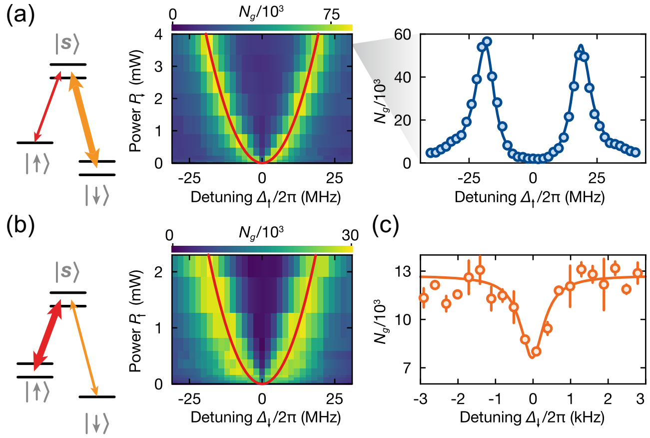

FIG. 2. Characterization of the Λ system. (a) Autler-Townes splitting probed on the $|\uparrow\rangle$–$|s\rangle$ transition in the presence of a strong resonant down-laser field, as illustrated by the level scheme. The color scale indicates the number of atoms that decayed into $|g\rangle$ through $^3P_1$ after excitation to $|s\rangle$. The blue data points show an example of a spectrum for fixed down-laser power $P_\downarrow = 3.6$ mW, which is fitted with an electromagnetically induced transparency model [31] (blue line) to extract the level splitting of $|s\rangle$. The red line represents a fit of the level splittings used to calibrate the one-photon Rabi frequency of the down transition. (b) The analog calibration of the one-photon Rabi frequency of the up transition. (c) Excitation spectrum at low coupling strength with resonant up-laser field. A Lorentzian fit (solid line) to the narrow dip in the data with a full width at half maximum of $2\pi \times 0.71(19)$ kHz demonstrates a large degree of coherence in our system.

differential light shifts. After driving two-photon Rabi oscillations with frequency Ω for a variable time t, we perform a state-selective readout of atoms in $|\uparrow\rangle$. For this purpose, we perform another Landau-Zener sweep to transfer the population from $|\uparrow\rangle$ to $|g\rangle$. We then detect the number of atoms in $|g\rangle$ in a spatially resolved manner with absorption imaging on the $^1S_0$–$^1P_1$ transition, as shown in Fig. 3(a). We achieve a detection fidelity of atoms in $|\uparrow\rangle$ of $(95.7 \pm 2.8)\%$, currently limited by the efficiency of the Landau-Zener sweep [22]. We repump any remaining atoms in $|\uparrow\rangle$ and remove them from the trap. This procedure leads to less than 1% contamination of the $|\downarrow\rangle$ population with atoms from $|\uparrow\rangle$. Then, we detect the number of atoms in $|\downarrow\rangle$ by repumping them to $|g\rangle$ via $|s\rangle$ using both Raman lasers. We take another absorption image and estimate a detection fidelity for atoms in $|\downarrow\rangle$ of $(95.9 \pm 3.3)\%$ [22].

When we analyze the Rabi frequencies spatially resolved, we find a variation of the Rabi frequencies due to the finite beam size of the Raman lasers in the yz-plane, see Fig. 3(b). To minimize the influence on the dephasing of the Rabi oscillations, we analyze the data at one spatial location [22]. To correct for long-term drifts of the atom number, we interleave reference measurements of the atom number in the initial state $|\uparrow\rangle$, which we use to normalize the population in $|\uparrow\rangle$ and $|\downarrow\rangle$ [22]. We observe high-contrast Rabi oscillations in $|\uparrow\rangle$, as shown in Fig. 3(c). For a

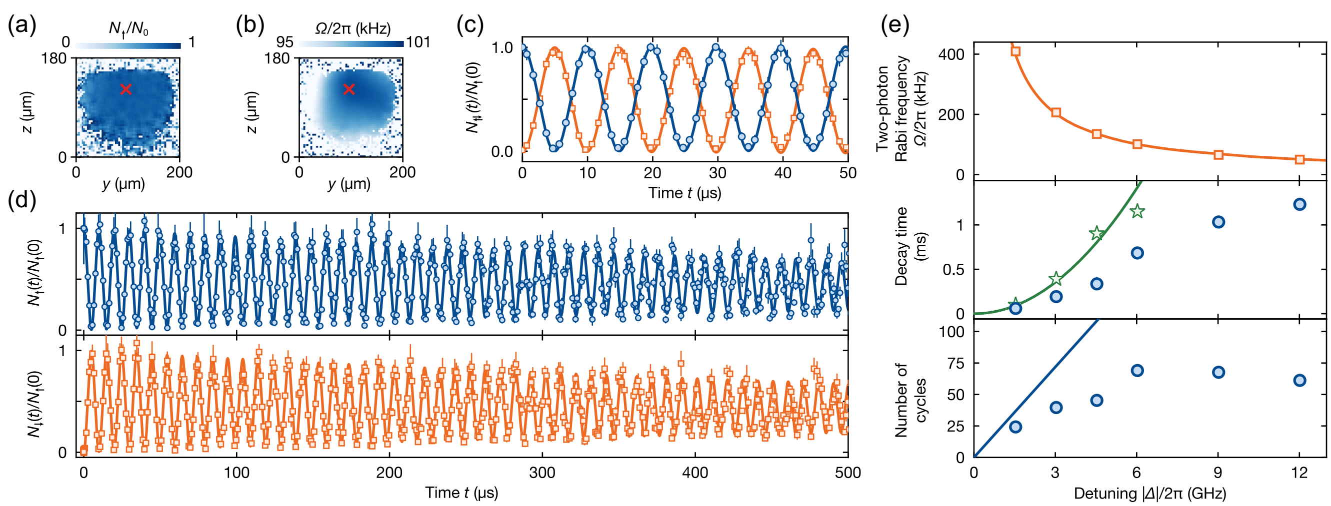

FIG. 3. Fine-structure qubit Rabi oscillations. (a) Measurement of the spatial distribution of the number of atoms in $|\uparrow\rangle$. (b) Spatial distribution of two-photon Rabi frequency Ω. The data for the Rabi oscillations are taken at the red cross. (c) Rabi oscillations with Raman lasers about $2\pi \times 6$ GHz red-detuned from $|s\rangle$. Blue circles (orange squares) show the number of atoms $N_\uparrow(t)$ and $N_\downarrow(t)$ in $|\uparrow\rangle$ and $|\downarrow\rangle$, respectively, both normalized with interleaved measurements of $N_\uparrow(0)$ and averaged over 10 experimental runs. The lines are fits with a sinusoidal oscillation. (d) A similar measurement as shown in (c), with data from individual runs of the experiment. The lines represent a damped sinusoidal-oscillation model illustrating that $\Omega = 2\pi \times 100.92(4)$ kHz and the exponential decay time $\tau = 0.68(1)$ ms, both found with our analysis method [22], provide a good description of the data. The error bars correspond to the standard deviation of the data in a 3×3 pixel region. (e) Rabi oscillations at various one-photon detunings $|\Delta|/2\pi$. Upper panel: the Rabi frequency (orange squares) shows a $1/\Delta$ dependence (orange line). Middle panel: The $1/e$ decay time τ of the envelope of the oscillations (blue dots) increases with Δ. The green stars and the solid line show the limit of the decay time given by the one-photon scattering rate. Lower panel: the number of cycles $\Omega\tau/(2\pi)$ (dots) increases with Δ and saturates at about 69 cycles (see text). The blue line shows the scattering-limited number of cycles inferred from the fits in the upper and middle panels.

π pulse with duration of about 5 μs, we find an excitation fraction of 98(1)% [22], without including the state-detection efficiencies above.

Next, we investigate the long-term dynamics of the Rabi oscillations, as shown in Fig. 3(d). To this end, we analyze the data to extract both carrier frequency and envelope of the oscillations in $|\uparrow\rangle$ separately. We determine the carrier frequency corresponding to Ω from a Lorentzian fit to the Fourier transform of the data [22]. Then, we apply a bandpass filter around Ω and detect the envelope of the Rabi oscillations. We fit the envelope of the filtered data with an exponential function to find the $1/e$ decay time τ of the envelope [22]. An exponentially damped sinusoidal-oscillation model based on Ω and τ obtained from this analysis method yields good agreement with our data of both qubit states, as shown in Fig. 3(d) [22].

Now, we study the influence of the one-photon detuning Δ on the Rabi oscillations, see Fig. 3(e). We measure Rabi frequencies up to $\Omega = 2\pi \times 409(1)$ kHz and find an expected scaling of the Rabi frequency as $\Omega \propto 1/\Delta$. The resulting decay times τ at small Δ are limited predominantly by one-photon scattering, which we characterize with independent measurements of the scattering rate, see middle panel of Fig. 3(e) [22]. We find that the number of cycles increases with $|\Delta|$ and saturates at about 69 cycles, as shown in the lower panel of Fig. 3(e) [22]. The scaling of τ with Ω and the saturation to 69 cycles is consistent with a residual inhomogeneity of Ω on the order of 0.4%, presumably caused by laser intensity noise and residual spatial inhomogeneity. We note that effects due to laser intensity noise could be strongly suppressed with standard composite pulse sequences [36].

Finally, to investigate the qubit coherence we perform Ramsey and spin-echo experiments, see Figs. 4(a) and 4(b). We use a one-photon detuning of about $2\pi \times 6$ GHz and apply a $\pi/2$ pulse to prepare a coherent superposition state $(1/\sqrt{2})(|\uparrow\rangle + |\downarrow\rangle)$. After a dark time T, we map the coherence onto population oscillations by varying the phase of a second $\pi/2$ pulse. In Fig. 4(c), we show the decay of the Ramsey contrast with increasing T. From a Gaussian fit to the data, we extract a $1/e$ dephasing time of $T_2^* = 2.03(7)$ ms, limited by residual differential light shifts of the nonmagic vertical lattice.

To quantify this light shift, we measure the change in the $|\uparrow\rangle$–$|\downarrow\rangle$ transition frequency as a function of the vertical potential depth using Ramsey spectroscopy. Contrary to the Ramsey measurements above, we do not scan the phase of the second $\pi/2$ pulse, but the dark time T between the pulses. The Raman laser frequencies are set to a two-photon detuning of $\delta \approx 2\pi \times 10$ kHz with respect to the free-space resonance of the qubit. The differential light shift that the atoms experience in the lattice causes an additional change in δ. The frequency of the resulting Ramsey oscillations f_{Ramsey} is equal to $\delta/(2\pi)$ and is extracted from a fit with a sinusoidal function, see Fig. 4(d). Figure 4(e) shows the

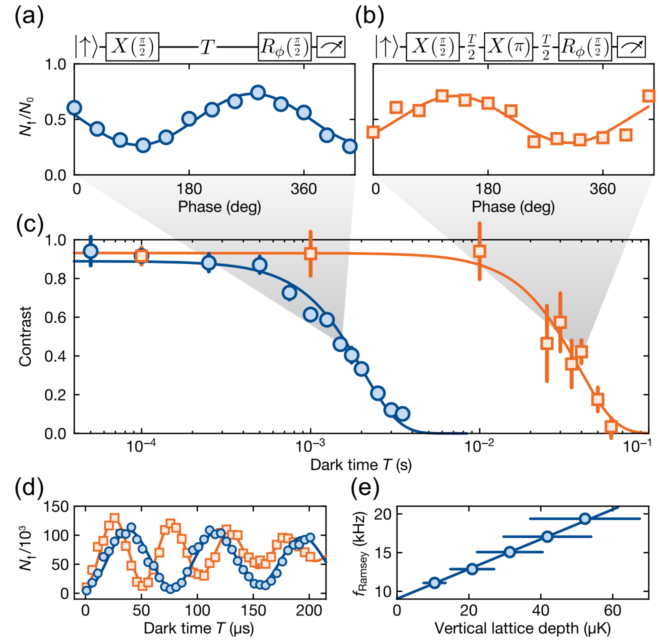

FIG. 4. Coherence measurements of the Sr fine-structure qubit. (a) Ramsey measurement. Two $\pi/2$ pulses at $|\Delta| = 2\pi \times 6$ GHz are applied with a dark time T in between. The phase of the second $\pi/2$ pulse is scanned. The resulting oscillations of the $|\uparrow\rangle$ population (dots) are fitted with a sinusoidal function (line). (b) Spin-echo measurement. A π pulse at $T/2$ lets the spins rephase at T. (c) Ramsey (blue dots) and spin-echo (orange squares) measurements for various T. We extract the contrast from the fits in (a) and (b) and fit a Gaussian decay with $1/e$ decay times of $T_2^* = 2.03(7)$ ms (blue line) and $T_2' = 38(3)$ ms (orange line) limited by the about 3 μK deep nonmagic vertical lattice. (d) Ramsey fringes as a function of T to extract the differential lattice light shift for vertical potential depths of 21 (6) μK (blue dots) and 52(15) μK (orange squares), as experienced by $|\uparrow\rangle$. The Raman lasers are tuned to a two-photon detuning of about $2\pi \times 10$ kHz with respect to the free-space resonance. The frequency f_{Ramsey} of the $|\uparrow\rangle$ population oscillations over the dark time T is determined with a damped sinusoidal fit model (lines). (e) f_{Ramsey} for different vertical potential depths of $|\uparrow\rangle$. A linear fit yields a differential light shift of 192(82) Hz/μK between $|\uparrow\rangle$ and $|\downarrow\rangle$ at the lattice-light wavelength of 1064 nm.

dependence of the Ramsey frequency on the vertical potential depth. A linear fit to the data extracts a differential light shift of 192(82) Hz/μK between $|\uparrow\rangle$ and $|\downarrow\rangle$ at a vertical lattice wavelength of 1064 nm, corresponding to a differential polarizability of about 1%.

To reduce dephasing caused by this differential light shift and other slow fluctuations present in the system, we carry out spin-echo measurements. We add a π pulse after $T/2$ to the Ramsey sequence, which lets the spins rephase at T. With this method, we extend the contrast decay time to $T_2' = 38(3)$ ms, as shown in Fig. 4(c). We project an additional order-of-magnitude increase in coherence time in a 3D magic lattice, supported by our recent results for the $|g\rangle$ and $|\uparrow\rangle$ states [20].

In summary, we demonstrated a new fine-structure qubit encoded in metastable Sr operating at a qubit splitting of 17 THz. We presented coherence times of tens of milliseconds, orders of magnitude longer than the single qubit gate times on the microsecond scale. Extending the coherence times further by an order of magnitude should be possible by modifying the currently limiting wavelength of the vertical lattice [19,20]. Particularly promising is a trapping wavelength of 813 nm, at which, based on our experimental results, we predict a triple magic condition for both qubit states and the ground state [19,22]. In such a configuration, the ${}^1S_0$–${}^3P_0$ clock transition and the ${}^1S_0$–${}^3P_2$ transition, used here for coherent transfer, could serve as additional tools for state-selective shelving operations and midcircuit readout. Moreover, the manipulation of the all-optical qutrit ${}^1S_0$–${}^3P_0$–${}^3P_2$ will be possible. Alternatively, operation at a triple-magic trap wavelength for the fine-structure qubit states and a particular Rydberg state might prove beneficial for reaching high two-qubit gate fidelities [15,16]. Also, fast state-selective readout of the fine-structure qubit states without the requirement of a slow shelving pulse can be implemented using the $5s5d\,{}^3D$ states [37,38]. Recently demonstrated imaging [39,40], resorting [41,42], and qubit addressing methods [43] enable individually addressable Sr qubits and can be combined with the methods presented here. Our results thus establish the Sr fine-structure qubit as an promising candidate for quantum computing, because it allows fast single-qubit rotations as well as high-fidelity two-qubit gates.

Note added.—In a study performed in parallel to ours, similar results have been achieved with atoms trapped in optical tweezers [44].

We thank M. Ammenwerth, F. Gyger, F. Meinert, T. Pfau, R. Tao, J. Trautmann, and J. Zeiher for stimulating discussions, S. Snigirev from planqc for support with experimental control hardware and software, and D. Filin and M. S. Safronova for providing the polarizability data. We acknowledge funding by the Munich Quantum Valley initiative as part of the High-Tech Agenda Plus of the Bavarian State Government, by the BMBF through the program "Quantum technologies—from basic research to market" (Grant No. 13N16357), and funding under the Horizon Europe program HORIZON-CL4-2022-QUANTUM-02-SGA via the project 101113690 (PASQuanS2.1). V. K. thanks the Hector Fellow Academy for support.

*sebastian.blatt@mpq.mpg.de

[1] M. Saffman, Quantum computing with atomic qubits and rydberg interactions: Progress and challenges, J. Phys. B **49**, 202001 (2016).

[2] C. Gross and I. Bloch, Quantum simulations with ultracold atoms in optical lattices, Science **357**, 995 (2017).

[3] L. Henriet, L. Beguin, A. Signoles, T. Lahaye, A. Browaeys, G.-O. Reymond, and C. Jurczak, Quantum computing with neutral atoms, Quantum **4**, 327 (2020).

[4] A. M. Kaufman and K.-K. Ni, Quantum science with optical tweezer arrays of ultracold atoms and molecules, Nat. Phys. **17**, 1324 (2021).

[5] A. W. Young, W. J. Eckner, W. R. Milner, D. Kedar, M. A. Norcia, E. Oelker, N. Schine, J. Ye, and A. M. Kaufman, Half-minute-scale atomic coherence and high relative stability in a tweezer clock, Nature (London) **588**, 408 (2020).

[6] I. S. Madjarov, J. P. Covey, A. L. Shaw, J. Choi, A. Kale, A. Cooper, H. Pichler, V. Schkolnik, J. R. Williams, and M. Endres, High-fidelity entanglement and detection of alkaline-earth Rydberg atoms, Nat. Phys. **16**, 857 (2020).

[7] N. Chen, L. Li, W. Huie, M. Zhao, I. Vetter, C. H. Greene, and J. P. Covey, Analyzing the Rydberg-based optical-metastable-ground architecture for ^{171}Yb nuclear spins, Phys. Rev. A **105**, 052438 (2022).

[8] A. Jenkins, J. W. Lis, A. Senoo, W. F. McGrew, and A. M. Kaufman, Ytterbium nuclear-spin qubits in an optical tweezer array, Phys. Rev. X **12**, 021027 (2022).

[9] J. W. Lis, A. Senoo, W. F. McGrew, F. Rönchen, A. Jenkins, and A. M. Kaufman, Midcircuit operations using the OMG architecture in neutral atom arrays, Phys. Rev. X **13**, 041035 (2023).

[10] W. Huie, L. Li, N. Chen, X. Hu, Z. Jia, W. K. C. Sun, and J. P. Covey, Repetitive readout and real-time control of nuclear spin qubits in ^{171}Yb atoms, PRX Quantum **4**, 030337 (2023).

[11] K. Barnes, P. Battaglino, B. J. Bloom, K. Cassella, R. Coxe, N. Crisosto, J. P. King, S. S. Kondov, K. Kotru, S. C. Larsen *et al.*, Assembly and coherent control of a register of nuclear spin qubits, Nat. Commun. **13**, 2779 (2022).

[12] S. Ma, A. P. Burgers, G. Liu, J. Wilson, B. Zhang, and J. D. Thompson, Universal gate operations on nuclear spin qubits in an optical tweezer array of ^{171}Yb atoms, Phys. Rev. X **12**, 021028 (2022).

[13] S. Ma, G. Liu, P. Peng, B. Zhang, S. Jandura, J. Claes, A. P. Burgers, G. Pupillo, S. Puri, and J. D. Thompson, High-fidelity gates and mid-circuit erasure conversion in an atomic qubit, Nature (London) **622**, 279 (2023).

[14] M. A. Norcia *et al.*, Midcircuit qubit measurement and rearrangement in a ^{171}Yb atomic array, Phys. Rev. X **13**, 041034 (2023).

[15] A. Pagano, S. Weber, D. Jaschke, T. Pfau, F. Meinert, S. Montangero, and H. P. Büchler, Error budgeting for a controlled-phase gate with strontium-88 Rydberg atoms, Phys. Rev. Res. **4**, 033019 (2022).

[16] F. Meinert, T. Pfau, and C. Hölzl, Quantum computing device, use, and method, eu patent application no. ep20214187.5 (2021).

[17] K. Toyoda, H. Shiibara, S. Haze, R. Yamazaki, and S. Urabe, Experimental study of the coherence of a terahertz-separated metastable-state qubit in ${}^{40}Ca^+$, Phys. Rev. A **79**, 023419 (2009).

[18] S. Haze, R. Yamazaki, K. Toyoda, and S. Urabe, Measurement and compensation of optical stark shifts for manipu-

lating the terahertz-separated qubit in $^{40}Ca^+$, Phys. Rev. A **80**, 053408 (2009).

[19] J. Trautmann, D. Yankelev, V. Klüsener, A. J. Park, I. Bloch, and S. Blatt, $^1S_0 - {}^3P_2$ magnetic quadrupole transition in neutral strontium, Phys. Rev. Res. **5**, 013219 (2023).

[20] V. Klüsener, S. Pucher, D. Yankelev, J. Trautmann, F. Spriestersbach, D. Filin, S. G. Porsev, M. S. Safronova, I. Bloch, and S. Blatt, Coherent excitation of a μHz scale optical magnetic quadrupole transition, arXiv:2401.03934.

[21] A. J. Park, J. Trautmann, N. Šantić, V. Klüsener, A. Heinz, I. Bloch, and S. Blatt, Cavity-enhanced optical lattices for scaling neutral atom quantum technologies to higher qubit numbers, PRX Quantum **3**, 030314 (2022).

[22] See Supplemental Material at http://link.aps.org/supplemental/10.1103/PhysRevLett.132.150605 for detailed methods and additional information, which includes Refs. [23–27].

[23] J. A. Boyd and T. Lahaye, A basic introduction to ultrastable optical cavities for laser stabilization, Am. J. Phys. **92**, 50 (2024).

[24] M. Beyreuther, R. Barsch, L. Krischer, T. Megies, Y. Behr, and J. Wassermann, ObsPy: A PYTHON toolbox for seismology, Seismol. Res. Lett. **81**, 530 (2010).

[25] E. R. Kanasewich, *Time Sequence Analysis in Geophysics* (University of Alberta, Edmonton, Alberta, Canada, 1981).

[26] S. Kuhr, W. Alt, D. Schrader, I. Dotsenko, Y. Miroshnychenko, A. Rauschenbeutel, and D. Meschede, Analysis of dephasing mechanisms in a standing-wave dipole trap, Phys. Rev. A **72**, 023406 (2005).

[27] F. Le Kien, P. Schneeweiss, and A. Rauschenbeutel, Dynamical polarizability of atoms in arbitrary light fields: General theory and application to cesium, Eur. Phys. J. D **67**, 92 (2013).

[28] P. Lemonde and P. Wolf, Optical lattice clock with atoms confined in a shallow trap, Phys. Rev. A **72**, 033409 (2005).

[29] A. Traverso, R. Chakraborty, Y. N. Martinez de Escobar, P. G. Mickelson, S. B. Nagel, M. Yan, and T. C. Killian, Inelastic and elastic collision rates for triplet states of ultracold strontium, Phys. Rev. A **79**, 060702(R) (2009).

[30] S. H. Autler and C. H. Townes, Stark effect in rapidly varying fields, Phys. Rev. **100**, 703 (1955).

[31] M. Fleischhauer, A. Imamoglu, and J. P. Marangos, Electromagnetically induced transparency: Optics in coherent media, Rev. Mod. Phys. **77**, 633 (2005).

[32] B. D. Agap'ev, M. B. Gornyĭ, B. G. Matisov, and Y. V. Rozhdestvenskiĭ, Coherent population trapping in quantum systems, Phys. Usp. **36**, 763 (1993).

[33] E. Arimondo, *V Coherent Population Trapping in Laser Spectroscopy* (Elsevier, New York, 1996), pp. 257–354.

[34] R. Finkelstein, S. Bali, O. Firstenberg, and I. Novikova, A practical guide to electromagnetically induced transparency in atomic vapor, New J. Phys. **25**, 035001 (2023).

[35] A. Heinz, A. J. Park, N. Šantić, J. Trautmann, S. G. Porsev, M. S. Safronova, I. Bloch, and S. Blatt, State-dependent optical lattices for the strontium optical qubit, Phys. Rev. Lett. **124**, 203201 (2020).

[36] D. Bluvstein, H. Levine, G. Semeghini, T. T. Wang, S. Ebadi, M. Kalinowski, A. Keesling, N. Maskara, H. Pichler, M. Greiner *et al.*, A quantum processor based on coherent transport of entangled atom arrays, Nature (London) **604**, 451 (2022).

[37] A. J. Daley, M. M. Boyd, J. Ye, and P. Zoller, Quantum computing with alkaline-earth-metal atoms, Phys. Rev. Lett. **101**, 170504 (2008).

[38] S. Stellmer and F. Schreck, Reservoir spectroscopy of $5s5p\ {}^3P_2$–$5snd\ {}^3D_{1,2,3}$ transitions in strontium, Phys. Rev. A **90**, 022512 (2014).

[39] R. Tao, M. Ammenwerth, F. Gyger, I. Bloch, and J. Zeiher, High-fidelity detection of large-scale atom arrays in an optical lattice, arXiv:2309.04717.

[40] S. Buob, J. Höschele, V. Makhalov, A. Rubio-Abadal, and L. Tarruell, A strontium quantum-gas microscope, arXiv:2312.14818.

[41] M. A. Norcia *et al.*, Iterative assembly of ^{171}Yb atom arrays in cavity-enhanced optical lattices, arXiv:2401.16177.

[42] F. Gyger, M. Ammenwerth, R. Tao, H. Timme, S. Snigirev, I. Bloch, and J. Zeiher, Continuous operation of large-scale atom arrays in optical lattices, arXiv:2402.04994.

[43] D. Bluvstein *et al.*, Logical quantum processor based on reconfigurable atom arrays, Nature (London) **626**, 58 (2024).

[44] G. Unnikrishnan, P. Ilzhöfer, A. Scholz, C. Hölzl, A. Götzelmann, R. K. Gupta, J. Zhao, J. Krauter, S. Weber, N. Makki, H. P. Büchler, T. Pfau, and F. Meinert, following Letter, Coherent control of the fine-structure qubit in a single alkaline-earth atom, Phys. Rev. Lett. **132**, 150606 (2024).